Fragmentation pathways and mechanisms of aromatic compounds in atmospheric pressure studied by GC–DMS and DMS–MS

Shai Kendler [a,b,*], Gordon R. Lambertus [a], Barry D. Dunietz [a], Stephen L. Coy [c],
Erkinjon G. Nazarov [c], Raanan A. Miller [c], Richard D. Sacks [a]

[a] *Department of Chemistry, University of Michigan, 930 North University Avenue, Ann Arbor, MI 48109, USA*
[b] *Department of Physical Chemistry, Israel Institute for Biological Research, 24 Lerer Street, P.O. Box 19, Ness-Ziona 74100, Israel*
[c] *Sionex Corporation, 8-A Preston Court, Bedford, MA 01730, USA*

Abstract

Differential mobility spectrometry (DMS) is a highly sensitive sensing technology capable of selecting and detecting ions based on the difference between ion mobility at high and low electric field. The combination of a micro-fabricated DMS with gas chromatography (GC) has allowed extensive investigation of the ion chemistry and collisionally induced dissociation (CID) of diaryl molecules on a millisecond timescale at temperatures up to $130\,^{\circ}C$. DMS-pre-filtered time-of-flight mass spectrometry (DMS–MS) has been used to verify the chemical composition of the ion species resolved by GC–DMS. This work focuses on the fragmentation of diaryl compounds, including diphenyl methane (DPM) and bibenzyl (BB), using information from the DMS and DMS–MS spectra of a series of aromatic compounds. Density functional theory calculations have been used to investigate the geometry and the energy along the reaction coordinate for the loss of benzene from $DPM \cdot H^+$ and $BB \cdot H^+$ for comparison with GC–DMS and DMS–MS experimental results and with previously reported chemical ionization MS. $DPM–H^+$ is observed to undergo field-induced fragmentation in the DMS to produce $C_7H_7^+(Bz^+)$ and unobserved neutral benzene with a low energy barrier. In contrast, $BB \cdot H^+$ fragments to $C_8H_9^+$ and benzene with a higher energy barrier. Calculated barriers and experimental results are in qualitative agreement. Depletion of the ionized fragments in favor of ion-neutral clusters was also observed at higher concentrations. It is suggested that CID in DMS can further enhance DMS analytical performance.

© 2007 Elsevier B.V. All rights reserved.

Keywords: DMS; Mobility; Fragmentation; Aromatic compound

1. Introduction

Emission of aromatic hydrocarbons from sources such as motor vehicles and industrial processes, poses a serious health risk to human populations especially in urban areas [1]. On-site detection of these compounds is important for understanding the migration of pollutants through the atmosphere [2] and for minimizing occupational exposure risks [3]. In the recent years, there has been an increasing effort towards the miniaturization of detection systems and their critical components such as gas chromatography (GC) columns and sensors [4–11]. Those efforts are aimed towards the development of highly portable and affordable systems. However, shrinking the size of analytical devices may result in degradation in performance. Cooks and co-workers explored the possibility of micro-fabricating an array of 10^6 miniature cylindrical ion trap mass analyzers in order to benefit from the reduction in power consumption while maintaining the ion capacity of a conventional ion trap MS [8]. Linear ion mobility spectrometer (IMS) is a sensitive detector that operates under atmospheric pressure, making it attractive for on-site analysis. Furthermore, IMS is a fast non-scanning analyzer which is advantageous in combination with on-site fast GC devices [12]. Ramsey and co-workers studied the sensitivity-limiting space charge effect caused by miniaturization of linear ion mobility spectrometer [9]. Pfeifer and Rumpf studied the effects of gate time, electric field magnitude and total charge on the ion pulse shape in a 12 mm diameter, 57 mm

* Corresponding author at: Department of Physical Chemistry, Israel Institute for Biological Research, 24 Lerer Street, P.O. Box 19, Ness-Ziona 74100, Israel. Tel.: +972 8 9381457; fax: +972 8 9381743.

E-mail address: ykendler@yahoo.com (S. Kendler).

length low temperature co-fired ceramic IMS drift tube [13]. Both these studies show that confining the ions into a compact pulse in time and space results in an increase in space charge effects which degrade the IMS resolving power. Recently, a micro-fabricated differential mobility spectrometry (DMS) (also known as field asymmetric ion mobility spectrometer—FAIMS) was developed and its applicability for on-site detection of organic compounds was demonstrated [14–18]. DMS shows good potential for miniaturization as it operates in continuous mode and can increase selectivity by increasing applied fields, with analysis times in the sub-millisecond range being quite feasible, both of which become easier as dimensions are reduced.

The theory and mechanisms governing separation in DMS were explored by several groups [19–26] DMS can be coupled to a variety of ionization sources. Radioactive ionization, corona discharge ionization, capacitive discharge ionization and UV photo-ionization have all been used in DMS. For the radioactive ^{63}Ni beta source used in this work, the dominant mechanism for ionization of the analyte is atmospheric-pressure chemical ionization (APCI), through proton transfer or charge transfer from positive and negative reactant ions. These reactant ions are conventionally called the positive reactant ion peak (RIP) and negative RIP. Positive RIP ions are observed in DMS mass spectrometric measurements at low humidity to consist of $(H_2O)_nH^+$ ($n = 0–3$) and N_2H^+, and negative RIP ions are observed as oxygen anion and a water-clustered oxygen anion (32 and 50 Da). Because the separate RIP masses are not resolved in DMS, the RIP ions are best regarded as proton–water–nitrogen clusters in the case of the positive RIP, and as oxygen anion–water clusters for the negative RIP [27]. The effects of temperature and humidity on APCI and the benefits of using of alternative reactant ions, have also been reported [24,25,28–31]. Ions exit the ionization chamber and are carried in a stream of gas through an analytical region to a pair of biased collector electrodes used to collect the positive and the negative ions from the same experiment. While carried by the gas stream, ions are subjected to an RF-frequency alternating asymmetric electrical field (dispersion voltage—DV). Since ion mobility at high electrical fields ($E > 10,000$ V/cm) depends on the field, alternating between high and low field changes the ion mobility, deflecting ions to the walls where they are neutralized. By applying an additional dc compensation voltage (CV), ion trajectories are modified to remain in the center of the cell, allowing them to reach the collector plates. The DMS spectrum of the sample is recorded by measuring the ion intensity as a function of CV and DV. The dependence of the ion mobility on the electrical field is described by [32]:

$$K\left(\frac{E}{N}\right) = K(0) + \left(1 + \alpha\left(\frac{E}{N}\right)\right)$$
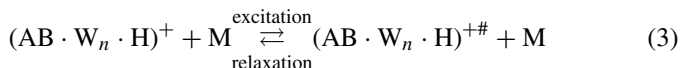$$= K(0)\left(1 + \sum_{k=1}^{N}\alpha_{2k}\left(\frac{E}{N}\right)^{2k}\right) \tag{1}$$

where $K(0)$ is the mobility of the analyte at low field conditions, α_{2k} are analyte-dependent coefficients and E/N is the ratio

between the electric field and the gas density measured in Td units ($1\,\text{Td} = 1 \times 10^{-17}\,\text{V cm}^2$). Eq. (1) is useful for relating molecular mobility values to results from different experimental configurations and for extracting mobility values from particular experimental results; however, it does not provide physical reasoning for the field effect on the ion mobility. One useful approximation may be obtained from momentum theory [32]:

$$K(E) = \frac{q}{N}\left(\frac{1}{2\mu k T_{\text{eff}}}\right)^{1/2}\frac{1}{\Omega(T_{\text{eff}})}, \tag{2}$$

where q is the ion electrical charge, μ the reduced mass, k the Boltzmann's gas constant, T_{eff} the effective temperature and $\Omega(T_{\text{eff}})$ is a momentum transfer effective collision cross-section.

Planar DMS is unique among differential mobility configurations in that very high electric fields are routinely applied, giving a wide range of effective temperatures. Planar DMS can achieve peak E/N over 200 Td, depending on pressure, with fields up to 30 kV/cm [33]. Collisions between the ions and neutrals at high electric fields result in internal excitation of the ion which may then relax at low fields:

$$(\text{AB} \cdot \text{W}_n \cdot \text{H})^+ + \text{M} \underset{\text{relaxation}}{\overset{\text{excitation}}{\rightleftarrows}} (\text{AB} \cdot \text{W}_n \cdot \text{H})^{+\#} + \text{M} \tag{3}$$

where M is the bath gas, W the water molecule and $(\text{AB}\cdot\text{W}_n\cdot\text{H})^{+\#}$ is a vibrationally excited ionic species. Determining the field-dependent distribution of ion-neutral collision energies requires sophisticated theoretical models, but the mean collision energy and the corresponding effective temperature are known to be well represented by [32]:

$$\tfrac{3}{2}kT_{\text{eff}} = \tfrac{3}{2}kT + \tfrac{1}{2}M_w v_{\text{d}}^2 = \tfrac{3}{2}kT + \tfrac{1}{2}M_w(KE)^2 \tag{4}$$

where M_w is the mass of the neutral. For two of the molecules discussed in the work, diphenyl methane (DPM) and bibenzyl (BB), the field-induced increase in effective temperature for DV of 1500 V is approximately 300 K above the DMS temperature (see last term in Eq. (4), $K \sim 1.7\,\text{cm}^2/\text{V.s}$). Much higher temperature increase (up to 3000 K) was reported for ions, having higher mobility, such as Cl^- [34]. The excited analyte ions might neutralize due to dissociation of the cluster ion or by electron detachment resulting in decrease in the ion flux. Unimolecular dissociation may also occur [35]:

$$(\text{AB}\cdot\text{W}_n\cdot\text{H})^{+\#} \rightarrow (\text{AB}\cdot\text{W}_n\cdot\text{H})^+ + \text{B} \tag{5}$$
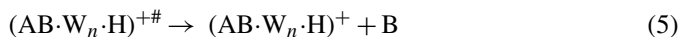
Miller et al. have shown that ion/molecule clustering at low fields followed by de-clustering at high field, results in an increase in differential ion mobility [14], due to changes in ion mass and collision cross-section. Thus, fragment ion/molecule clustering should be taken into consideration at high concentration of neutral polyatomic molecules. Collisionally induced dissociation (CID) of peptides and proteins in linear IMS has been reported recently by Clemmer and co-workers [36–38]. The ions are excited inside activation zones which were coupled to the IMS, before or after separation according to mobility. It was shown that the fragmentation pattern contains useful analytical information. Eiceman et al. studied the fragmentation of butylacetate isomers and found strong dependence

on the ion structure, while the temperature effect was less pronounced. At elevated temperatures (150 °C), the major fragment ions, obtained from *tert*-butyl and *iso*-butyl acetates were $[C_4H_9]^+$ and was protonated acetic acid from *sec*-butyl acetate. No fragmentation was observed for *n*-butyl acetate [28]. With DMS on the other hand, both *n*-butyl and *n*-ethyl acetate fragmented at 100 °C [6], probably due to the elevated effective temperature obtained by ion acceleration in high electric fields (Eq. (4)).

The chemical reactivity of protonated aromatic molecules has been explored, mainly at low pressure, using mass spectrometry [39–44]. The dominant species upon protonation of the benzene ring is the σ-complex in which the extra hydrogen is attached to one of the carbon atoms. Hydrogen is seen to migrate rapidly between the aromatic ring carbon atoms ("ring walk") [45]. In diarenes (Ph(CH$_2$)$_n$Ph), protonation on the ipso site results in fragmentation according to [44,46]:

$$[AR(CH_2)_nAR{-}H]^+ \rightarrow AR(CH_2{}^+)_n + AR \tag{6}$$

Fragmentation products may also undergo other chemical reactions such as rearrangement, charge transfer and nucleophilic substitution.

This study deals with the fragmentation of diarene ions during separation in a micro-fabricated DMS. The effects of DMS temperature, dispersion voltage and analyte concentration on the fragmentation efficiencies and routes of diarenes are presented. Experimental results are compared to quantum chemical calculations. Enhancement of the analytical capabilities of the DMS through control of the fragmentation efficiency, in analogy to MS^n techniques, is also discussed.

2. Experimental

2.1. Chemicals

Samples for the GC/DMS experiments were prepared by dissolving 1–4 mg of the analytes in pentane (Acros, >99%). A list of the analytes, their purities and some physical properties are given in Table 1.

2.2. GC separation conditions

Liquid samples (0.2 μL) were injected to a heated split/splitless inlet mounted on a GC (Varian 3400, Palo Alto, CA). Split ratio was 1:50 and inlet temperature was 250 °C. The sample was vaporized in the inlet and separated on a 3 m long, 0.1 mm inner diameter capillary column coated with 0.1 μm polydimethylsiloxane (Restek Corp., Bellefonte, PA). All chromatographic separations were done under isothermal condition at 110 °C with carrier gas flow rate of 0.5 mL/min (99.99999% pure nitrogen Cryogenic Gases, Detroit, MI). Carrier gas was further purified prior to use by filtration through a molecular sieve/drierite trap followed by a liquid nitrogen cold trap. Evaluations of the concentration effects on the relative ratio of the peak heights for a component were done under conditions where the chromatographic peaks were intentionally broadened by lowering the carrier gas flow rate to 0.2 mL/min and setting the oven temperature to 75 °C. These changes generated peak widths between 30 and 60 s for the targeted species.

2.3. DMS design

The differential mobility spectrometer is composed of an ionization region, which houses a 5 mCi ^{63}Ni ionization source, a tunable ion filter, and collector electrodes, as seen in Fig. 1. Ions formed in the ionization region by APCI are passed in a stream of transport gas (99.99999% pure nitrogen from Cryogenic Gases, which was further purified as described earlier) through the ion filter region composed of two planar parallel electrodes. Pressure in the DMS is ambient atmospheric pressure, monitored and recorded through the instrument software by an internal pressure sensor. The exposed electrode dimensions in the ion filter region are 15 mm × 1.0 mm, and the gap between them is 0.5 mm. Filtered ions are detected downstream from the filter by two electrically biased electrodes connected to detection circuits that measure the current due to ions that pass through the ion filter. DV frequency for the asymmetric waveform is ∼1.2 MHz with peak amplitude controlled between 500 and 1500 V. The compensation voltage can be set or scanned within the range from −43 to +15 V. The controlling Sionex

Table 1
List of chemicals, purities and physical properties

Analyte name	Abbreviation	BP (°C)	Purity (%)	Source	Proton affinity (kJ/mol[a])	MW (g/mol)
Benzene	B	80.3	99.5	Alfa Aesar	750.4	78.11
Toluene	TOL	110.8	99.5	Spectrum	784.0	92.14
p-Xylene	pXYL	138	>99	Aldrich	794.4	106.17
m-Xylene	mXYL	138	98	Aldrich		106.17
o-Xylene	oXYL	144	97	Aldrich	796	106.17
Cycloheptatriene	CHT	116	90	Acros Organics	833	92.14
Styrene	STY	146	>90	Fisher Chemicals	839.5	104.15
Indene	IND	181	99	Alfa Aesar	848.8	116.16
Ethylbenzene	EB	136	99.8	Aldrich	788.0	106.17
Propylbenzene	PB	159	98	Aldrich	790.1	120.2
Diphenyl methane	DPM	262	99	Acros Organics	802.0	168.23
Bibenzyl	BB	283	99	Acros Organics	801.8	182.26

[a] Proton affinity of CHT was obtained from Ref. [51]; other proton affinities were obtained from Ref. [52].
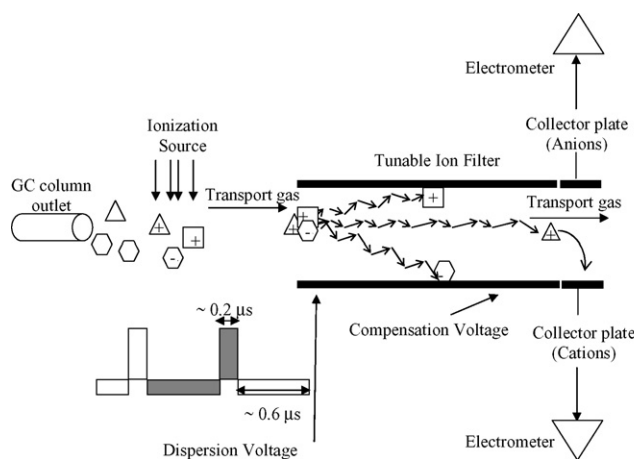
Fig. 1. An overview of the micro-fabricated DMS apparatus. More details regarding the separation process are given in the text.

Expert software presents the data as color topographical plots of positive or negative ion current as a function of CV for each GC retention time and as individual CV scans at the current DV voltage. Parameters selected by the user include CV scanning parameters (range, step size and rate), DV amplitude, DMS temperature, and transport gas flow rate (200–500 sccm). Typically, the CV was scanned from −12 to 8 V in 0.04 V steps within one second. Unless otherwise noted, transport gas flow rate was 300 mL/min, resulting in a residence time of 1.5 ms in the ion filter.

2.4. DMS/MS design

Mass spectroscopic identification of ions observed in DMS was made using a Sionex DMS mass spectrometric pre-filter unit mounted on a JEOL Accutof time-of-flight mass spectrometer. This pre-filter uses the Sionex microDMx^{TM} planar DMS design. DMS dispersion and compensation voltages are used to select specific ions into the mass spectrometer inlet. CV scans or coupled DV–CV scans are synchronized with Accutof data acquisition. The pre-filter can operate at temperatures to 130 °C, at pressures from 0.4 to 1.4 atm, and exhibits peak widths in CV units on the order of 0.7 V [47].

In using the DMS–MS interface to identify ion masses, mass spectrometer inlet conditions are adjusted to minimize fragmentation in the pressure transition region from near-atmospheric pressures to vacuum. DMS conditions in the pre-filter region (DV, CV, temperature, pressure) were selected to allow identification of the differential mobility features under the conditions used in GC–DMS.

2.5. Computational methods

Optimized and transition state molecular structures their energies and vibrational frequencies were calculated using Q-Chem 3 package [48], at B3LYP/6-311G** level of theory. All optimized structures had only positive vibrational frequencies, while the transition state geometries had one imaginary frequency.
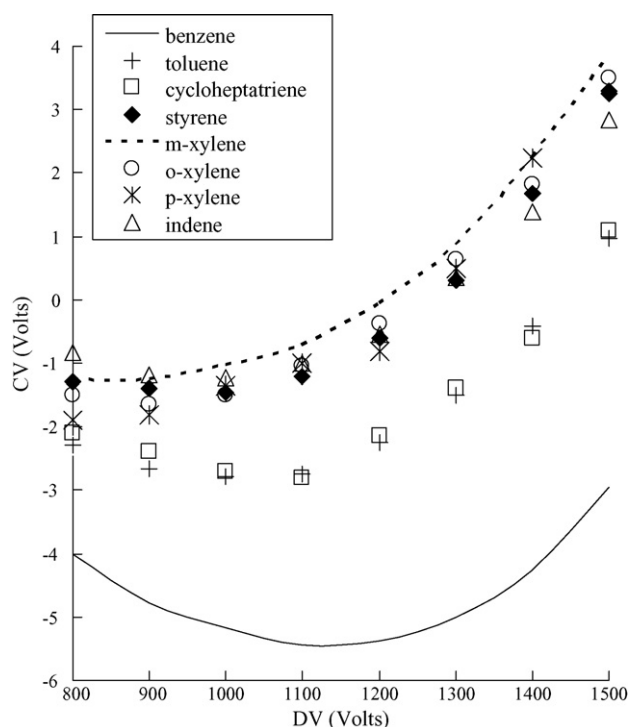

Fig. 2. The compensation voltage as a function of the dispersion voltage ("dispersion plot") for several aromatic compounds, at 100 °C.

3. Results and discussion

3.1. Experimental results

Fig. 2 shows the relationship between the DMS dispersion and compensation voltages (dispersion plot) of several aromatic compounds at DMS temperature of 100 °C.

Dispersion curves show the DMS compensation voltage required for maximum transmission of a selected ion through the ion filter region of the DMS at a particular dispersion voltage. The required (CV, DV) values for maximum transmission are directly related to the field dependence of the ion mobility ($\alpha(E/N)$ in Eq. (1)) in a well-known way, and are determined by the chemical identity and conformation of the ion species. Ion transmission values through the filter region are represented as maximum transmission curves in Figs. 2 and 3, but ion transmission may also be represented as color-coded topographic-style dispersion plots with CV and DV axes as is done in Figs. 4 and 5. All of these compounds show similarly shaped but displaced dispersion curves and CV scans at fixed DV show a single peak that dominates the DMS response. Peak widths (FWHM) were about 1 V. The uncertainty due to GC–DMS repeatability in CV values (σ_{CV}) was determined from the standard deviation of repeated GC–DMS measurements, typically $\sigma_{CV} = 0.3$ V. Similar measurements were performed for DPM and BB, Fig. 3 shows the dispersion plots obtained for DPM and BB at DMS temperature of 100 °C. For DPM and for BB two peaks were obtained. These peaks are marked as DPM[1], DPM[2], BB[1] and BB[2]. The CV values, measured for DPM[2], are more negative than those measured for DPM[1] and are close but not identical

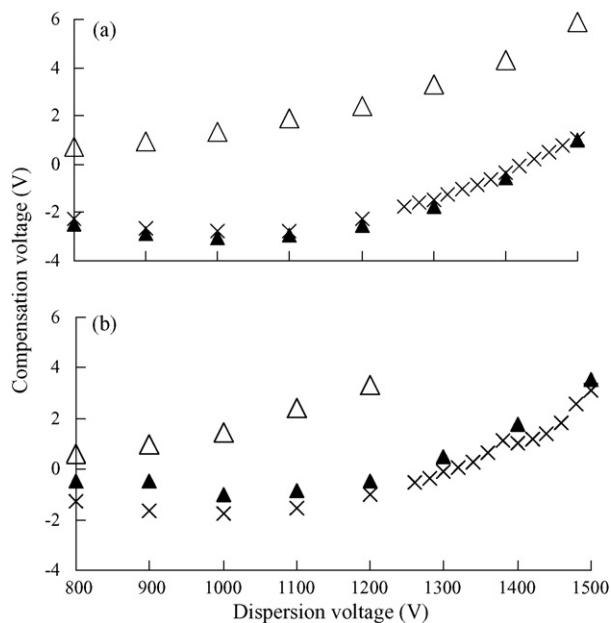Fig. 3. Dispersion plots of diphenyl methane (DPM) and bibenzyl (BB). For both molecules two peaks were obtained: (a) DPM^1 ($\triangle$) and DPM^2 ($\blacktriangle$) in comparison to toluene ($\times$), and (b) BB^1 ($\triangle$) and BB^2 ($\blacktriangle$) in comparison to ethylbenzene ($\times$). DMS temperature was 100 °C and mass flow was 0.1 ng/s.

between $3\sigma_{CV}$ at DV = 800–1000 V and $2\sigma_{CV}$ at DV = 1200–1500 V.

DMS-pre-filtered TOF mass spectrometry has been used to improve the understanding of the underlying ion chemistry of DPM and BB. The DPM peak was identified as [C$_7$H$_7$]$^+$ (m/z = 91 a.m.u.) which results from the fragmentation of DPM·H$^+$ to benzilium cation (Bz$^+$) and neutral benzene, the known fragmentation products of DPM·H$^+$. The DPM^1 peak at high temperature and low field was identified as a mixture of the four ionic species including DPM·H$^+$, DPM$^+$, DPM·Bz$^+$ and DPM·Bz$^+$–C$_6$H$_6$. At DMS temperature lower than 60 °C this mixture was further resolved by DMS. Fig. 4 shows results obtained with the DMS and with DMS–MS for a mass flow of 1.8 ng/s of DPM at 60 °C, with both DV and CV scanned. C$_7$H$_7^+$(Bz$^+$) begins to appear at DV = 800 V and increases in intensity as DV increases, while DPM·H$^+$ intensity decreases with DV and disappears at DV > 1200 V. As the Bz$^+$ signal increases, two other species appear having composition [DPM·Bz$^+$–C$_6$H$_6$] (m/z ∼ 181 a.m.u.) and [DPM·Bz$^+$] (∼259 a.m.u.) by exact mass. It is suggested that these ion–molecule adducts are formed due to collisions between Bz$^+$ and the neutral molecule in the DMS since it was found that decreasing the neutral DPM level caused the 181 and 259 a.m.u. peaks to disappear—further study of the mass flow effect on the ion abundances will be given later.

The results for BB are similar to those obtained DPM. Fig. 5 shows the results obtained with DMS and with the DMS-pre-filtered MS at 100 °C as a function of the DV. Loss of a benzene moiety from the protonated parent molecule occurs at DV values higher than 800 V and the parent ion is totally depleted at
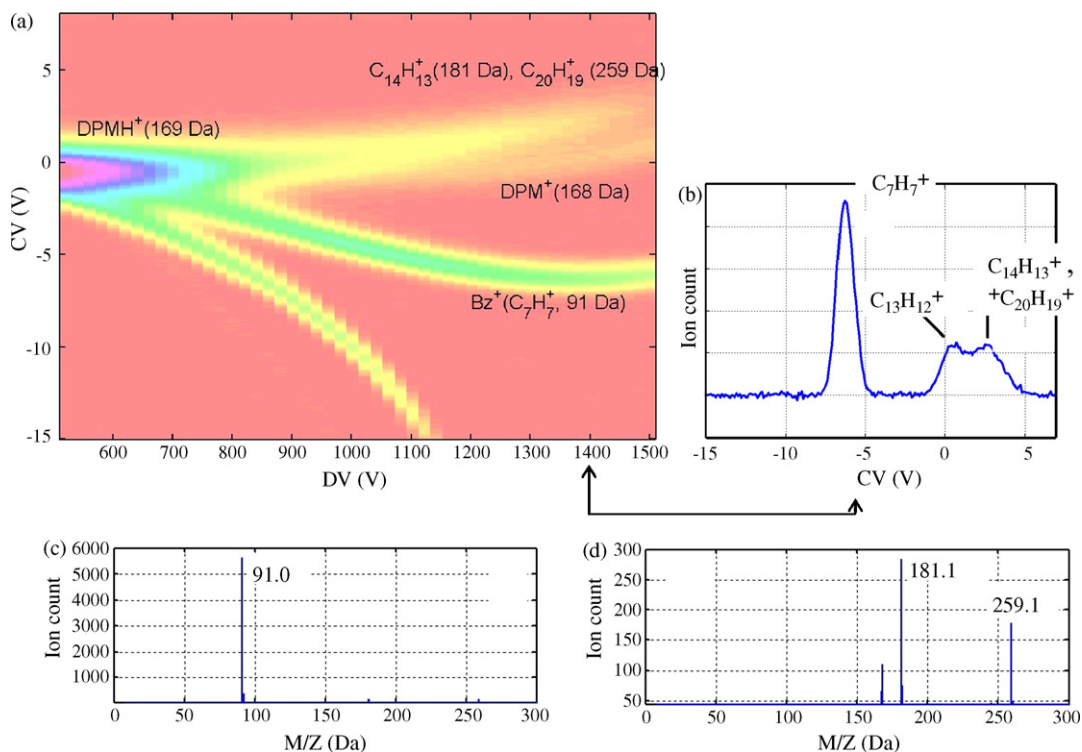
to those measured for toluene (also shown in Fig. 3a). The difference between CV(DPM^2) and CV(toluene) is lower than the repeatability uncertainty, σ_{CV}. In the case of BB, at DV > 1200 V the peak BB^1 disappears. The difference between CV values of BB^2 and those of protonated EB (also shown in Fig. 3b) varies

Fig. 4. Dispersion plot DPM at 60 °C in N$_2$ carrier gas with DMS–MS identifications (a); a CV scan from the dispersion plot at DV = 1400 V (b); DMS–MS analysis at DV = 1200 V and CV = −5.2 V (c); DMS–MS analysis at DV = 1200 V and CV = −0.3 V (d). Experiments were performed at mass flow of 1.8 ng/s of DPM.
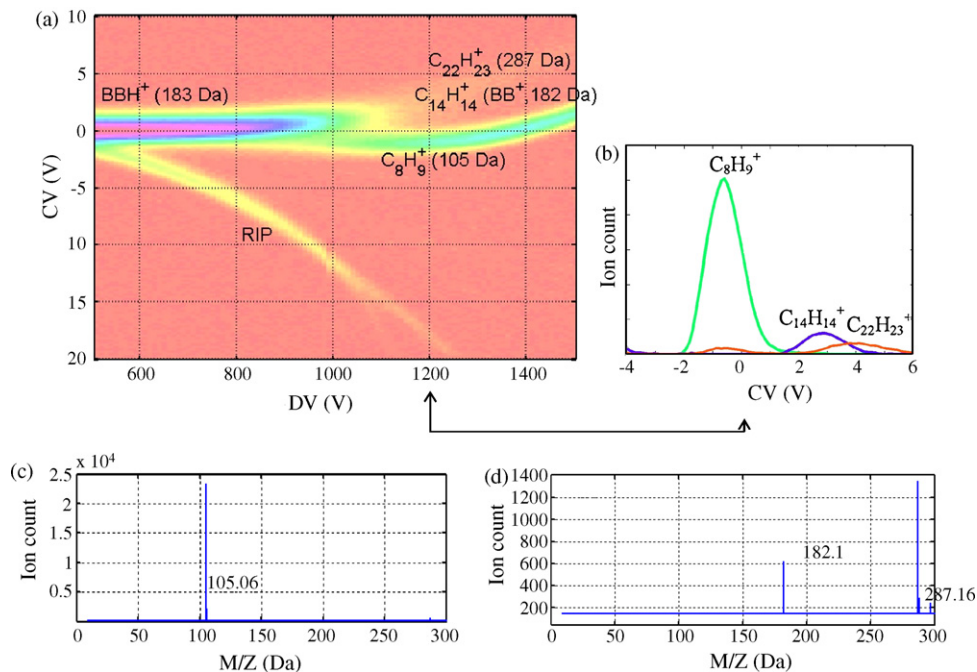
Fig. 5. DMS dispersion plot of bibenzyl (BB) at 100 °C in N_2 carrier gas with DMS–MS identifications (a); mass resolved DMS plot at DV = 1200 V (b); DMS–MS mass analysis at DV = 1200 V and CV = −0.6 V (c); DMS–MS mass analysis at DV = 1200 V and CV = 4.1 V (d). At this temperature cluster ion signal (m/z = 287 a.m.u.) is partially resolved from BB (182 a.m.u.). Experiments were performed at mass flow of 10 ng/s of BB.

DV values higher than 1200 V. The resulting fragment ion was identified as $[C_8H_9]^+$ (m/z = 105 a.m.u. $(EB–H)^+$) and, as mentioned earlier, requires a different CV than that for protonated ethylbenzene $[C_8H_{11}]^+$ (m/z = 107 a.m.u.). The difference in ion mobility or effective cross-section for these two ions of masses

105 and 107 a.m.u. underlines the fact that several molecular properties in addition to mass modify ion mobility and differential ion mobility values, as has been previously demonstrated for leucine/isoleucine [49] and for several geometrical isomers of substituted olefins [50].
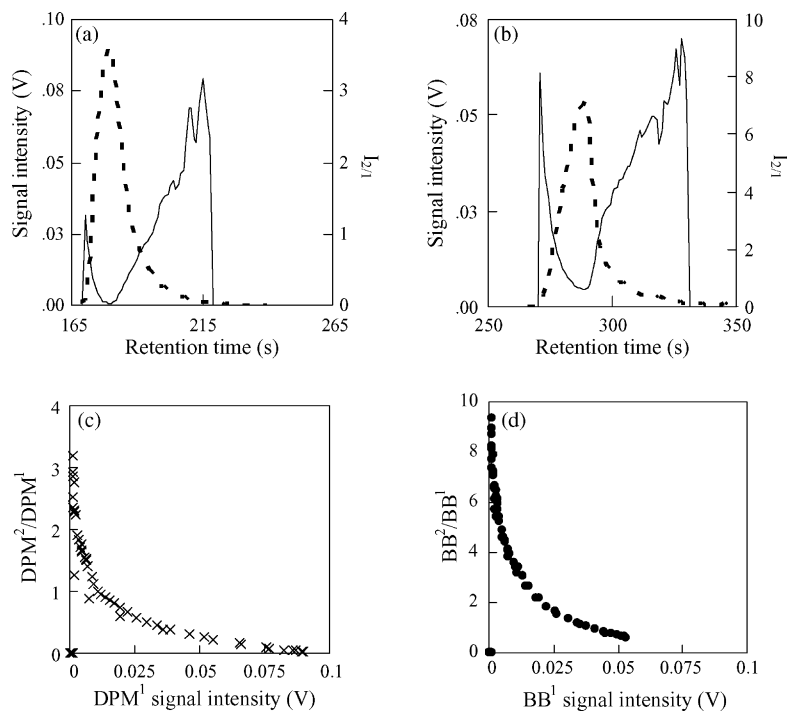
Fig. 6. Chromatogram recorded for DPM^1 (dashed line left axis) and $I_{2/1}$ (solid line right axis) (a) and same for BB (b). $I_{2/1}$ as a function $I[DPM^1]$ (c) and the same for BB (d). DMS temperature was 100 °C, DV amplitude = 1200 V, average mass flow was 1 ng/s, $CV[DPM^1]$ = 2.25 V, $CV[DPM^2]$ = −2.4 V, $CV[BB^1]$ = 3.2 V and $CV[BB^2]$ = −0.3 V.

The appearance of DPM$^+$ and BB$^+$ ("M$^+$") was not expected in these APCI experiments. It was found that the abundance of the M$^+$ species was almost unaffected by the DV, and was linear with the analyte mass flow. The possibility that "M$^+$" is created due to reaction involving more than one analyte molecule was investigated by reducing the DPM concentration to a point where cluster ions are no longer detected, yet the DPM$^+$ signal persisted. Similar experiments were performed with toluene vapor. In these experiments, [toluene]$^+$ as well as [toluene·H]$^+$ were detected. The formation of M$^+$ in these experiments could be due either to direct electron-impact ionization (EI) or to charge transfer between the aromatic molecules and an electron acceptor such as N$_2$$^+$ or NO$^+$ (observed as a minor RIP species in these experiments, and as a cluster with toluene).

Fragmentation efficiency as a function of DV amplitude and DMS temperature was studied. During those measurements It has been noticed that the ratio $I_{2/1} = I[M^2]/I[M^1]$ (M = DPM or BB) is affected by the analyte mass flow. This behavior was studied by injecting DPM and BB samples into the GC, which was operated at conditions where the chromatographic peaks are broad (FWHM = 30–60 s, see Section 2 for more detail). With

extended elution times from the GC, the intensity of the fragment ion can be monitored at several different mass flows in a single experiment. Signal intensities were obtained by averaging the signal of individual ionic species along the CV axis over the CV range at which the peak occurs. The baseline offset was subtracted prior to the calculation. Averaging the signal improved the signal-to-noise ratio by about a factor of four, yielding noise levels of ~1 mV. Fig. 6 shows the effect of analyte mass flow on the $I_{2/1}$ ratios of DPM and BB. For both analytes, $I_{2/1}$ goes down as M^1 goes up. This behavior is evident in the chromatograms (Fig. 6a and b) and in plots of $I_{2/1}$ as a function of $I[M^1]$ (Fig. 6c and d). Similar results were obtained in multiple experiments, performed at different analyte mass flows. For these additional mass-flow experiments, $I_{2/1}$ was calculated from the ratio between $I[M^2]$ and $I[M^1]$ at the maximum of the M^2 chromatographic peak. Fig. 7 shows the results of two GC/DMS measurements performed at average mass flows of 1 and 0.1 ng/s. These results are attributed to the formation of clusters between fragment ions (Bz$^+$ and C$_8$H$_9$$^+$) and the neutral molecules (DPM or BB), as observed in DMS/MS measurements. Formation of these adducts is reduced at the lower concentrations which occur at the front or tail of chromatographic peaks. At the chromatographic peak, the fragment ions almost disappear due to complete complexation with neutrals. In light of this mass flow effect, the influence of the DV amplitude and DMS temperature on the fragmentation efficiency was evaluated at low mass flows. This was achieved by analyzing the GC peak for $I[M^2]$ and $I_{2/1}$, as describe earlier (Fig. 6c and d), only at low $I[M^1]$ intensities ranging between

Fig. 7. GC/DMS separation and detection of DPM and BB. The horizontal axis shows the compensation voltage (CV) and the vertical axis shows the retention time (second), ion intensity is given in a color-code (see color scale on the right hand of the figure). Measurements were performed with analyte mass flow of: 1 ng/s (a) and 0.1 ng/s (b). DMS temperature was 100 °C, DV = 1200 V and transport gas flow was 300 sccm.
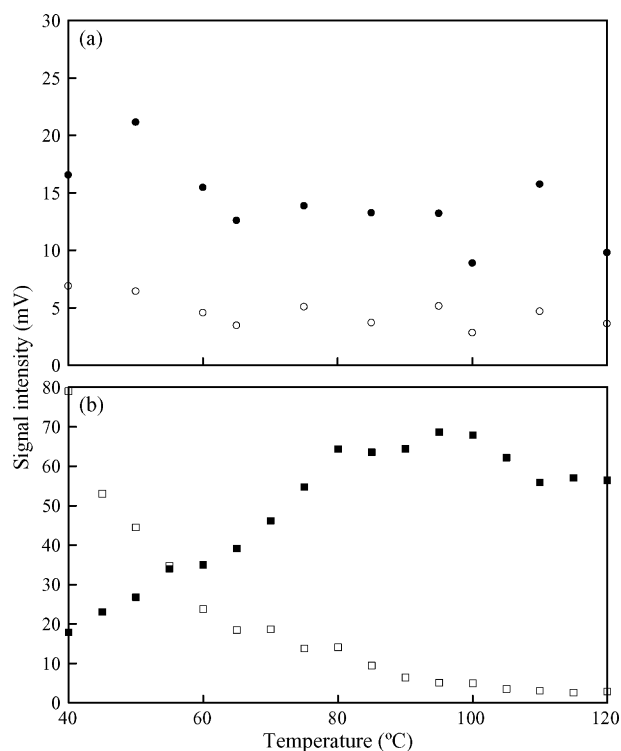

Fig. 8. The effect of DMS temperature at DV amplitude of 1300 V on the signal intensity of DPM^1 (○) and DPM^2 (●) (a), and on the signal intensity of BB^1 (□) and BB^2 (■) (b).
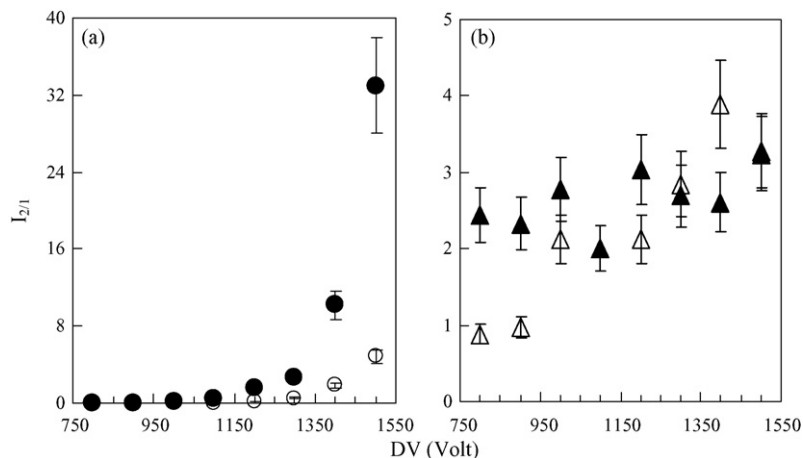
Fig. 9. The effect of DV amplitude on $I_{2/1}$ of BB at 75 °C ($\bullet$) and 50 °C ($\bigcirc$) (a), and on DPM at 75 °C ($\blacktriangle$) and 50 °C ($\triangle$) (b).

2 and 4 mV, which corresponds to signal-to-noise ratio (SNR) ratios of 2–4.

Fig. 8 shows the effect of temperature on the signal intensities of DPM and BB fragmentation product at DV amplitude of 1300 V. Ion signals in DMS vary slightly with the temperature due to changes in mobility and diffusion rates even for non-reactive molecules and more significantly due to changes with temperature in charge competition with reactant ion species. As an approximate compensation for these effects, signal intensities were normalized to the ion signal of benzene, which increases by factor two approximately as temperature increases from 40 to 120 °C. With this normalization, Bz[+] signal intensity is almost constant at DV = 1300 V between 40 and 120 °C. DPM[1] signal intensity is also constant at that temperature range (Fig. 8a). MS measurements performed at the CV_{DPM1} showed that DPM·H^{+} is totally depleted at these conditions and the main species at this CV is DPM[+] which is not seen to fragment on this millisecond time scale.

In contrast to DPM, for BB it was found that increasing DMS temperature from 40 to 120 °C increased fragment ion intensity and decreased BB[1]. Although BB[1] does not disappear, even at high temperature, the dominant species in the BB[1] CV range changes from BB·H^{+} to BB[+] as BB·H^{+} is fragmented (see Fig. 5). Similar results were obtained for DMS temperatures of either 50 or 75 °C with DV amplitude scanned between 800 and 1500 V (Fig. 9). BB fragmentation efficiency shows strong dependence on the DV amplitude while DPM fragmentation efficiency is practically constant at 75 °C, and increases only by factor four at 50 °C. Furthermore, DPM is fragmented even at DV = 800 V and T = 50 °C, while BB starts to fragment only above DV = 1100 V at 75 °C, and DV = 1200 V at T = 50 °C. The weak dependence of DPM fragmentation efficiency on the DMS temperature and DV amplitude is in accord with the reaction scheme suggested by Kuck and Bäther [44] and Kuck et al. [45]. According to this scheme, the intra-annular hydrogen-walk is fast both in BB and DPM, allowing the protons to spread randomly among the various ring sites (para, ortho, meta and ipso). Dissociation occurs from the ipso site with a very low energy barrier for DPM and with much higher barrier for BB [44,45]. Since the fragmentation barrier

for DPM is low, it is expected that the temperature dependence of fragmentation efficiency will be low. It is also expected that the fragmentation efficiency will be higher than that of BB.
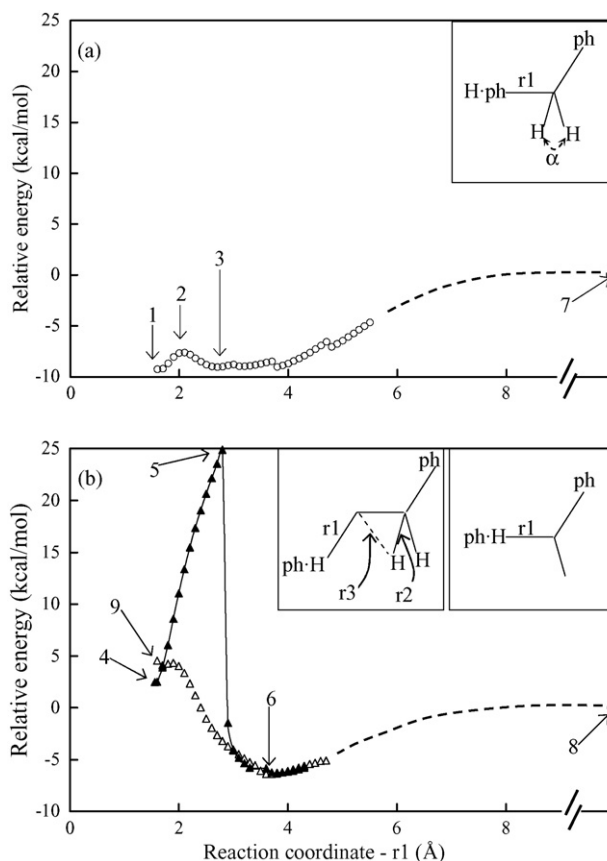

Fig. 10. Energy profile along the reaction coordinate (r_1) of $[DPM·H]^+_{ipso}$ ($\bullet$) (a), $[BB·H]^+_{ipso}$ ($\blacktriangle$) and protonated 1,1-diphenyl ethane $[DPM·H]^+_{ipso}$ ($\triangle$) (b). Energy was set to zero for the fragmentation product at infinite separation. Energy profile was calculated for $[DPM·H]^+_{ipso}$ up to $r_{1max} = 5.5$ Å; 4.3 Å for $[BB·H]^+_{ipso}$ and 4.7 Å for $[DPM·H]^+_{ipso}$, the dashed line is for guidance. Structures of species 1–9 indicated in the graphs, are given in Table 2. The insets show also the bond lengths and angle (r_1, r_2, r_3, α) that showed significant change along the reaction coordinate – see Table 2.
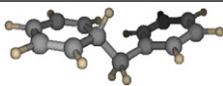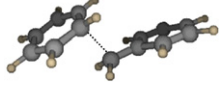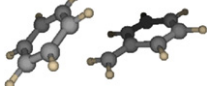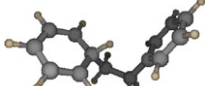
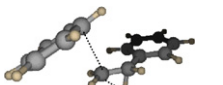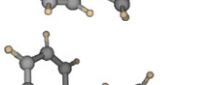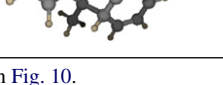### 3.2. Calculated results

The equilibrium structures for DPM·H$^+$ and BB·H$^+$ and the energetics underlying the benzene-loss reaction for both species were calculated. The lowest energy structure was found by performing the energy minimization calculation starting from different geometries ("initial guesses"). In these initial guess, the proton was attached to a different carbon atom in the aromatic ring and in the methyl group. Since the aromatic ring can rotate around the C–C sigma bond for each protonation site several different rotamers were considered. For [DPM·H]$^+$ two structures, having similar energy, were found. In one rotamer, the aromatic rings are perpendicular ("PE") to each other; in the other rotamer, the two rings are facing ("FA") each other. At equilibrium, the proton is located at the para position in both rotamers. For BB·H$^+$ the most stable species is the FA, where the proton is located at the ortho position. Upon protonation on the ipso position only one structure for both [DPM·H]$^+$ and [BB·H]$^+$ was obtained (species numbers 1 and 4 in Table 2). Next, the reactivity of the ipso protonated DPM and BB species was analyzed.

Fig. 10 shows the relative energy profile of [DPM·H]$^+$, [BB·H]$^+$ and protonated 1,1-diphenyl ethane [DPE·H]$^+$, along the reaction coordinate, which is the C$_{ipso}$–C$_{methylene}$ bond length (r_1). This potential-energy-surface (PES) was initially calculated by constrained optimization, with bond distance (r_1) parameterized. Therefore, the height of the energy barrier extracted from this PES can serve as an upper limit. The transition state (TS) predicted from the calculated PES at $r_1 = 2.8$ Å, was optimized (without any constrain) resulting in a similar geometry to that found in the parameterized optimization having $r_1 = 2.65$ Å. The optimized TS structure features a single imaginary frequency which is associated with the hydrogen transfer. Consequently, this TS structure has been verified to link the bonded BB·H$^+$ to the dissociation products, C$_8$H$_9^+$ and C$_6$H$_6$. Table 2 lists the important geometrical features of the different species along with graphical illustration of their structures. The predicted energy barrier for BB is 77.4 kJ/mol (ZPE corrected) in comparison to less than 4.1 kJ/mol (ZPE corrected) calculated for DPE·H$^+$. It is noted that the energy barrier for the dissociation of DPM is even lower than the barrier for fragmenting the ion–molecule cluster ([benzene–benzilium]$^+$, species number 3 in Fig. 10). The $m/z = 169$ peak is therefore assigned either to the ion–molecule cluster or to the protonated DPM where the proton is *not* located on the ipso site. A theoretical study dealing with the overall energetic and dynamics of proton migration in diaryl molecules is ongoing. It is also predicted that immediately *after* [BB·H]$^+$ crosses the transition state to [C$_8$H$_9$]$^+$ it rearranges by 1,2 H shift (PhCH$_2$CH$_2^+ \rightarrow$ PhCH$^+$CH$_3$). These findings are in accord with experimental results reported by Bäther and Grützmacher [46]. Significantly, this calculation locates the rearrangement along the reaction coordinate.

Table 2
Calculated structure of several species obtained during the fragmentation of [DPM·H]$^+$, [BB·H]$^+$ and [DPE·H]$^+$

Species number	Structure	Remarks[a]
1		[DPM·H]$^+$—hydrogen located at the ipso position, $r_1 = 1.6$ Å, $\alpha = 109°$
2		Transition state for the dissociation of [DPM·H]$^+$, $r_1 = 2.1$ Å, $\alpha = 115°$
3		[Benzene·benzilium]$^+$ cluster, bond length = 2.7 Å, $r_1 = 2.7$ Å, $\alpha = 117°$
4		[BB·H]$^+$—hydrogen located at the ipso position, $r_1 = 1.586$ Å, $r_2 = 1.095$ Å, $r_3 = 2.134$ Å
5		Transition state for the dissociation of [BB·H]$^+$, $r_1 = 2.65$ Å, $r_2 = 1.142$ Å, $r_3 = 1.845$ Å
6		[Benzene·CH$_3$CHPh]$^+$ cluster, $r_1 = 3.5$ Å, $r_2 = 1.109$ Å, $r_3 = 2.055$ Å
7 and 8		Fragmentation products, $r_1 = \infty$, $r_2 = 1.101$ Å, $r_3 = 2.083$ Å, $\alpha = 117°$
9		[DPEH]$^+$, $r_1 = 1.65$ Å

[a] r_1, r_2, r_3 and α are defined in Fig. 10.

The fact that fragmentation of $[DPM \cdot H]^+_{ipso}$ requires crossing a very low energy barrier suggests that the $[DPM \cdot H]^+$ signal intensity should be lower than that of $[BB \cdot H]^+$ under the same conditions. Indeed $[DPM \cdot H]^+$ signal is totally depleted at lower temperature and DV than $[BB \cdot H]^+$. It is emphasized that the calculated transition barriers refer to the reactive forms of both species, where the proton is located at the ipso site, as the reactant state.

4. Conclusions

Coupling micro-fabricated DMS to a gas chromatograph results in multidimensional separations that rely both on chromatographic retention times and also on differential mobility CV and DV, providing a highly sensitive and selective analytical tool. However, accurate analysis in the presence of interfering materials could require further enhancement of the resolving power. GC/DMS/DMS (DMS with field-induced fragmentation) can provide complimentary chemical information based on fragmentation patterns and the relative ratios of the parent and daughter peak heights as well as their dependence on DMS operational parameters—temperature, dispersion voltage and analyte mass flow.

Fragments ion intensities, generated from $[DPM \cdot H]^+$ and $[BB \cdot H]^+$, were found to be highly dependent on the mass flow of the analyte through the sensor. At higher mass flow, the signal intensity for the fragmented species decreases or disappears due to the formation of clusters between the fragment ion and neutrals. For this reason, temperature and dispersion voltage effects on the fragmentation efficiency were studied at mass flows close to the minimum detectable limit (approximating "infinite dilution").

Experimental results for $[DPM \cdot H]^+$ showed that fragmentation occurred under all detector operating conditions. For $[BB \cdot H]^+$, fragmentation was not induced until DV = 1100 V at 75 °C, and RF = 1200 V at $T = 50$ °C. These results prove that dissociation of $[BB \cdot H]^+$ involves crossing a high energy barrier while the energy barrier for the dissociation of $[DPM \cdot H]^+$ is much lower. Ions structures, proton affinities and the energetics underlying the fragmentation reactions were calculated using density functional theory (B3LYP/6-311G**). The calculated proton affinities were only 1–3% higher than the experimental value. As predicted from the experimental results, the calculated energy barrier for the dissociation of $[DPM \cdot H]^+$ is very low (4.1 kJ/mol), while that of $[BB \cdot H]^+$ is relatively high (77.4 kJ/mol). The calculated PES shows that the 1,2 H shift of the $[BB \cdot H]^+$ fragment ($[C_8H_9]^+$) occurs after the molecule crosses the transition state. The calculated results are in agreement with previously reported results obtained at reduced pressure using CI/MS.

Fragmentation patterns in MS/MS are frequently used for identification and structural analysis of unknown components and for the analysis of complex mixtures. Enhancement of the analytical capabilities of DMS utilizing CID—would be a significant step towards the realization of a completely micro-fabricated DMS/DMS spectrometric technique. This could be achieved in several ways, for example: the DMS could be operated at non-CID conditions until a suspected analyte is detected. Once it is detected, the dispersion voltage could be increased rapidly resulting in CID. An alternative approach might be splitting the sample between two micro-fabricated devices; one of the devices will be operated in non-CID conditions and the other at high temperature and dispersion voltage. In this way, the sample could be analyzed *simultaneously* in non-CID and CID conditions. In both ways, utilizing chromatographic techniques to pre-separate the sample is of great importance when complex samples are considered.

References

[1] M. Törnqvist, L. Ehrenberg, Environ. Health Perspect. 102 (Suppl. 4) (1994) 173.
[2] B. Rappenglück, P. Fabian, J. Appl. Meteorol. 38 (1998) 1448.
[3] G. Bieniek, S. Kurkiewicz, T. Wilczok, J. Occup. Health 46 (2004) 175.
[4] P.S. Dittrich, K. Tachikawa, A. Manz, Anal. Chem. 78 (12) (2006) 3887.
[5] P. Östman, L. Luosujärvi, M. Haapala, K. Grigoras, R.A. Ketola, T. Kotiaho, S. Franssila, R. Kostiainen, Anal. Chem. 78 (2006) 3027.
[6] G.R. Lambertus, C.S. Fix, S.M. Reidy, R.A. Miller, D. Wheeler, E. Nazarov, R.D. Sacks, Anal. Chem. 77 (2005) 7563.
[7] B.J. Shortt, M.R. Darrach, P.M. Holland, A. Chutjian, J. Mass Spectrom. 40 (2005) 36.
[8] M.G. Blain, L.S. Riter, D. Cruz, D.E. Austin, G. Wu, W.R. Plass, G.R. Cooks, Int. J. Mass Spectrom. 236 (2004) 91.
[9] J. Xu, W.B. Whitten, J.M. Ramsey, Anal. Chem. 72 (2000) 5787.
[10] S. Reidy, G.R. Lambertus, J. Reece, R. Sacks, Anal. Chem. 78 (2006) 2623.
[11] S. Kendler, S.M. Reidy, G.R. Lambertus, R.D. Sacks, Anal. Chem. 78 (19) (2006) 6765.
[12] J.P. Dworzanski, W.H. McClennen, P.A. Cole, S.N. Thornton, H.L.C. Meuzelaar, N.S. Arnold, A.P. Snyder, Field Anal. Chem. Technol. 1 (5) (1998) 295.
[13] K.B. Pfeifer, A.N. Rumpf, Anal. Chem. 77 (2005) 5215.
[14] R.A. Miller, E.G. Nazarov, G.A. Eiceman, A.T. King, Sens. Actuators A 91 (2001) 307.
[15] G.A. Eiceman, E. Krylov, N. Krylova, E.G. Nazarov, R.A. Miller, Anal. Chem. 76 (2004) 4937.
[16] G.A. Eiceman, E.V. Krylov, B. Tadjikov, R.G. Ewing, E.G. Nazarov, R.A. Miller, Analyst 129 (2004) 297.
[17] H. Schmidt, F. Tadjimukhamedov, I.V. Mohrenz, G.B. Smith, G.A. Eiceman, Anal. Chem. 76 (2004) 5208.
[18] R.A. Miller, E.G. Nazarov, U.S. Patent 6,495,823 (2002).
[19] M.P. Gorshkov, USSR Inventors Certificate No. 966583 (1982).
[20] I.A. Buryakov, E.V. Krylov, E.G. Nazarov, U.K. Rasulev, Int. J. Mass Spectrom. Ion Processes 128 (1993) 143.
[21] G.E. Spangler, R.A. Miller, Int. J. Mass Spectrom. 214 (2002) 95.
[22] R. Guevremont, R.W.J. Purves, Am. Soc. Mass Spectrom. 16 (2005) 349.

[23] A.A. Shvartsburg, K. Tang, R.D. Smith, J. Am. Soc. Mass Spectrom. 15 (2004) 1487.

[24] N. Krylova, E. Krylov, G.A. Eiceman, J.A. Stone, J. Phys. Chem. A 107 (2003) 3648.

[25] E. Krylov, E.G. Nazarov, R.A. Miller, B. Tadjikov, G.A. Eiceman, J. Phys. Chem. A 106 (2002) 5437.

[26] R Guevremont, J. Chromatogr. A 1058 (2004) 3.

[27] G.A. Eiceman, Z. Karpas, Ion Mobility Spectrometry, CRC Press, Boca Raton, FL, 1993.

[28] G.A. Eiceman, D.B. Shoff, C.S. Harden, A.P. Snyder, Int. J. Mass Spectrom. Ion Processes 85 (1988) 265.

[29] A.H. Lawrence, P. Neudorfl, Anal. Chem. 60 (1988) 104.

[30] K.A. Daum, D.A. Atkinson, R.G. Ewing, Talanta 55 (2001) 491.

[31] C.A. Hill, C.L.P. Thomas, Analyst 130 (2005) 1155.

[32] E.A. Mason, E.W. McDaniel, Transport Properties of Ions in Gases, Wiley, New York, 1988.

[33] E.G. Nazarov, S.L. Coy, E.V. Krylov, R.A. Miller, G.A. Eiceman, Anal. Chem. 78 (22) (2006) 7697.

[34] L.A. Viehland, E.A. Mason, At. Data Nucl. Data Tables 60 (1995) 37.

[35] C.A. Veasey, C.L.P. Thomas, Analyst 129 (2004) 198.

[36] S.J. Valentine, S.L. Koeniger, D.E. Clemmer, Anal. Chem. 75 (2003) 6202.

[37] S.I. Merenbloom, S.L. Koeniger, Valentine FS.J., M.D. Plasencia, D.E. Clemmer, Anal. Chem. 78 (2006) 2802.

[38] S.L. Koeniger, S.I. Merenbloom, S.I. Valentine, M.F. Jarrold, H.R. Udseth, R.D. Smith, D.E. Clemmer, Anal. Chem. 78 (12) (2006) 4161.

[39] J.A. Herman, A.G. Harrison, Org. Mass Spectrom. 16 (1981) 423.

[40] D. Kuck, Mass Spectrom. Rev. 9 (1990) 583.

[41] B. Chiavarino, M.E. Crestoni, S. Fornarini, J. Phys. Org. Chem. 17 (2004) 957.

[42] M.E. Crestoni, S. Fornarini, D. Kuck, J. Phys. Chem. 99 (1995) 3150.

[43] D. Kuck, D. Thölmann, H.F. Grützmacher, J. Chem. Soc. Perkin Trans. 2 (1990) 251.

[44] D. Kuck, W. Bäther, Org. Mass Spectrom. 21 (1986) 451.

[45] D. Kuck, W. Bäther, H.-F. Grützmacher, Int. J. Mass Spectrom. Ion Processes (1985) 67–75.

[46] W. Bäther, H.-F. Grützmacher, Int. J. Mass Spectrom. Ion Processes 64 (1985) 193.

[47] Details of the Sionex DMS/MS interface will be the subject of a future publication.

[48] Y. Shao, L.F. Molnar, Y. Jung, J. Kussmann, C. Ochsenfeld, S.T. Brown, A.T.B. Gilbert, L.V. Slipchenko, S.V. Levchenko, D.P. O'Neill, R.A. DiStasio Jr., R.C. Lochan, T. Wang, G.J.O. Beran, N.A. Besley, J.M. Herbert, C.Y. Lin, T. Van Voorhis, S.H. Chien, A. Sodt, R.P. Steele, V.A. Rassolov, P.E. Maslen, P.P. Korambath, R.D. Adamson, B. Austin, J. Baker, E.F.C. Byrd, H. Daschel, R.J. Doerksen, A. Dreuw, B.D. Dunietz, A.D. Dutoi, T.R. Furlani, S.R. Gwaltney, A. den Hey, S. Hirata, C. Hsu, G. Kedziora, R.Z. Khalliulin, P. Klunzinger, A.M. Lee, M.S. Lee, W. Liang, I. Lotan, N. Nair, B. Peters, E.I. Proynov, P.A. Pieniazek, Y.M. Rhee, J. Ritchie, E. Rosta, C.D. Shernll, A.C. Simmonett, J.E. Subotmk, H.L. Woodcock III, W. Zhang, A.T. Bell, A.K. Chakraborty, D.M. Chipman, F.J. Keil, A. Warshel, W.J. Hehre, H.F. Schaefer III, J. Kong, A.I. Krylov, P.M.W. Gill, M. Head-Gordon, Phys. Chem. Chem. Phys. 8 (2006) 3172.

[49] D.A. Barnett, B. Ells, R. Guevremont, R.W. Purves, J. Am. Soc. Mass Spectrom. 10 (1999) 1279.

[50] Z. Karpas, Anal. Chem. 61 (1989) 684.

[51] J.Y. Salpin, M. Mormann, J. Tortajada, M.T. Nguyen, D. Kuck, Eur. J. Mass Spectrom. 9 (2003) 361.

[52] E.P. Hunter, S.G. Lias, J. Phys. Chem. Ref. Data 27 (1998) 413.